Atomic Elemental and Chemical Analysis of $SrTiO_3/LaMnO_3$ Multilayers Using Fast Simultaneous EELS and EDS Analysis in DigitalMicrograph

Paolo Longo,[1]* Paul J Thomas,[1] Aziz Aitouchen,[1] Phil Rice,[2] Teya Topuria,[2] and Ray D Twesten[1]

[1]Gatan Inc., 5794 W Las Positas Blvd., Pleasanton, CA, 94588

[2]IBM Research Division, Almaden Research Center, San Jose CA, 95120

*plongo@gatan.com

Introduction

In an age of atomic-scale control of materials and interfaces, the need for high spatial resolution characterization of composition and local bonding is accelerating. Scanning transmission electron microscopy (STEM) based techniques continue to be the gold standard for such analysis at interfaces, and aberration correction of the STEM probe has extended this ability to atomic levels [1, 2]. The utility of this technique, however, is limited by the ability to detect the signals generated in the STEM. To confront this challenge, STEM-based electron energy loss spectrometers (EELS) and energy-dispersive (EDS) spectrometers have undergone improvements in efficiency and speed, enabling atomic-scale composition maps using EELS [3,4] and in some cases EDS [4, 5, 6, 7] for a range of materials. In addition, atomic-scale bonding maps using EELS fine structure are possible in certain selected systems.

In this article, we show how jointly acquired EELS and EDS data can extend the capability of each technique over the case when data are acquired alone. We use a system that links the acquisition of the otherwise independent EELS, EDS, and probe positioning systems. These disparate types of data are acquired in exact synchrony and with the fidelity of their native applications [8]. In our results here we show the level of $SrTiO_3/LaMnO_3$ interface data that can be captured with GIF Quantum atomic-scale mapping of compositional details over hundreds of unit cells at the interface. Zooming in at a particular imperfection at the interface, we have used the ability of EELS to detect changes in local bonding, as well as detection of interfacial diffusion at steps and the associated change in the bonding state of the metal atoms in the perovskite lattice.

Materials and Methods

Instrumentation. Data for this article were acquired at IBM, San Jose, CA, using a probe-corrected 200 kV STEM equipped with a cold FEG high-brightness source (JEM-ARM200F), including a large solid-angle SDD-EDS system. EELS data were acquired with a GIF Quantum® ER system, and spectrum imaging acquisition was with the high-speed STEMPack® for EELS and EDS [9]. The GIF Quantum ER is configured with the following features: (a) DualEELS capability, which allows the nearly simultaneous acquisition of two different regions of the EELS spectrum [3, 9, 10, 11]; (b) a low-dispersion mode that allows the acquisition of EELS data with an energy range up to 2,000 eV, which can be extended up to 4,000 eV when the data are acquired in DualEELS mode [9]; (c) a fast 2k×2k CCD, which allows the acquisition of EELS spectra at over 1,000 spectra per second [9]; and (d) a dodecapole-based lens system capable of correcting spectral aberrations up to the 5th order, allowing collection angles over 100 mrad and yet maintaining sub-eV energy resolution [9].

Test Specimen. The sample analyzed was a $SrTiO_3$ (STO)/$LaMnO_3$ (LMO) bilayer structure grown on an STO substrate. The bilayer was capped with STO, creating a buried STO/LMO/STO/LMO structure. The sample was prepared for TEM by conventional cross-sectioning, which involves cutting, grinding, dimpling, and Ar ion milling using a Gatan PIPS. This procedure ensures high-quality, relatively thin TEM specimens, which are free of the amorphous layer present in samples prepared using FIB as a result of the interaction of the Ga ion beam with the sample. This amorphous layer, even at the 1–2 nm level, often limits the quality of atomic-level analysis unless the lamella is re-polished with a lower-damage technique beforehand [12].

Acquisition Parameters. Data shown here were acquired using a STEM probe of about 200 pA measured using the pico-ammeter built in the drift tube in the GIF Quantum [9]. A probe convergence angle of 28 mrad and a collection angle of approximately 100 mrad were employed. Using a large collection angle for the EELS experiment provides a larger signal and also has some advantages in compositional mapping [13]. The collection solid angle of the detector used to acquire the EDS data was reported to be 0.98 sr, but this was not independently measured in the present experiments. The sample was tilted to the [001] zone axis, which caused the plane of the specimen to be tilted about 1° toward the EDS detector. Three different experiments were carried out with this setup: large-field-of-view mapping, high-speed simultaneous EELS/EDS acquisition, and detection of atomic-level bonding effects at an interphase interface. These are described below. For the fast mapping and compositional analysis experiments, the spectrometer was set up with an energy dispersion of 1 eV/channel. Such low dispersion has the advantage of giving a large field of view (2,000 eV) in the EELS spectrum and also the maximum amount of intensity in the CCD. The main disadvantage is the poor energy resolution that can be 3 eV at the best.

Results

Large field-of-view mapping at atomic resolution. Figure 1 shows a large field-of-view annular dark field (ADF)

https://doi.org/10.1017/S1551929515000589 Published online by Cambridge University Press

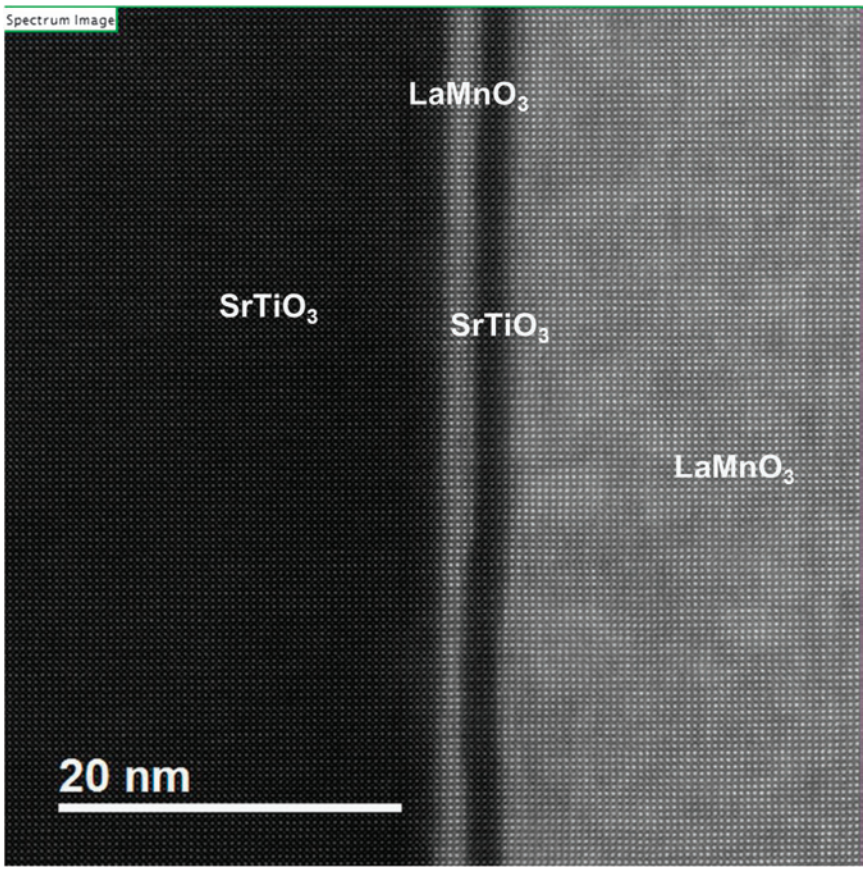

Figure 1: ADF STEM survey image. The EELS SI was taken across the region inside the green box that extends over the entire image.

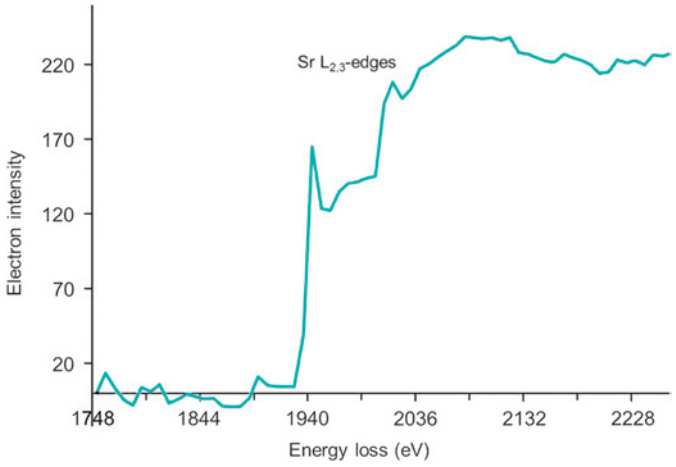

Figure 2: Background subtracted EELS spectrum of the Sr $L_{2,3}$-edges at 1,940 eV. Each EELS spectrum was acquired with only 1.5 ms exposure time. Despite the short exposure time per spectrum, the Sr L_3 and L_2 white lines can be observed.

image of atomic columns at the STO/LMO/STO/LMO interface. The interface appears abrupt in the upper portion of the image but is quite rough with the presence of terraces in the lower portion of the image indicating some growth in homogeneities. The high sensitivity of the CCD in the GIF Quantum allows the acquisition of EELS at high speed with good signal-to-noise ratio (SNR), and the high stability of the microscope installation at IBM allows compositional distribution analysis at the atomic level across the entire area shown in the ADF STEM image in Figure 1. The region was divided into 1,050×1,050 pixels, and EELS spectra were acquired at a rate of 500 spectra/second across the entire area. Each EELS spectrum was acquired using an exposure time of 1.5 ms. Even with such a short exposure time, the system is so sensitive that high-energy edges such as the Sr $L_{2,3}$ at 1,940 eV have good SNR, as shown in Figure 2. Given the very short exposure time used for the experiment, the spectrometer was set with the highest possible binning both in the non-dispersive (vertical at 130×) and the energy (horizontal at 8×) directions. Binning along the vertical direction does not affect the energy resolution, but there is a huge improvement in sensitivity and spectral readout speed. Notwithstanding the improvements in sensitivity, 8× binning along the horizontal (that is, energy) direction strongly deteriorates the energy resolution as the total number of energy channels reduces from 2,048 down to 256. However, in the case of compositional analysis, the signal is extracted over a wide energy integration range, thus the energy resolution is not very important. Figure 3a shows a colorized composite of the EELS elemental maps for Ti, Mn, La, and Sr (oxygen is omitted for clarity). Here it is possible to see that the interface becomes fairly irregular in the lower portion of the map as indicated in the ADF STEM image (Figure 1). However, by zooming in on one of terraces along the interface, it is possible to observe elemental diffusion that in some areas across the STO/LMO interface extends up to 2 monolayers, as indicated by the 2 arrows in Figure 3b. In addition, the interface seems to maintain its crystalline structure with the presence of atomic columns containing both La and Sr in one case and Mn and Ti in the other case. It is important to mention that no spatial drift correction was employed during the acquisition of the spectrum imaging (SI). Although some spatial distortion and minor drift can be seen, the single, continuous pass acquisition ensures fidelity of the composition maps.

Combined EELS and EDS results from fast elemental mapping analysis. EELS and EDS elemental maps were taken from a smaller region of the same interface of Figure 1. In this case, EELS data were acquired in single-range mode, and three different signals (ADF, EDS, and EELS core-loss) were recorded simultaneously. To ensure adequate counts in the EDS data, the spectrum integration time per pixel was increased to 10 ms compared to the 1.5 ms of the first example. The EELS spectrum was acquired from 300 eV to 2,300 eV, and the EDS spectra were acquired simultaneously, integrating counts over the entire pixel time employed for the EELS acquisition. The entire 180×80 pixel spectrum imaging dataset was acquired in just over 2 minutes.

Elemental maps were constructed from spectrum images for relevant EELS edges (Sr-L at 1,940 eV, Ti L at 456 eV,

LUMENCOR
CUSTOMER FOCUS

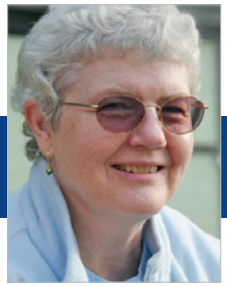

Aurelie Snyder
OHSU

OREGON HEALTH & SCIENCE UNIVERSITY

SEEING MORE with LESS

Your job is to assist and advise researchers in the use of advanced microscopy techniques, correct?

Yes, I am an imaging specialist at the Advanced Light Microscopy Core at The Jungers Center at Oregon Health Sciences University. It is a shared resource of high-end microscopy systems. I'm responsible for 10 microscope systems and support a user base of over 350 researchers and clinicians.

How have Lumencor's light engines impacted your work?

We installed a Lumencor light engine as part of our wide-field deconvolution imaging system. It replaced a metal halide light source. There was so much more intensity with the light engine that the speed of analysis was dramatically improved. Our data acquisition rates (frames per second) increased by a factor of 2 for fixed samples and by a factor of 4 for live cell samples. Illumination necessary to achieve a good image was reduced from hundreds of milliseconds to tens of milliseconds.

"Anybody who has struggled with phototoxicity problems in live cell imaging experiments will readily appreciate the benefits of being able to limit light exposure."

What are some other benefits that you and users of your facility have noticed?

The illumination is even across the field of view through the eyepieces, which is larger than that of the camera detection area. **An additional attraction is the rapid electronic switching between excitation channels,** providing a further decrease in acquisition speed compared to microscopes equipped with mechanical filter wheels.

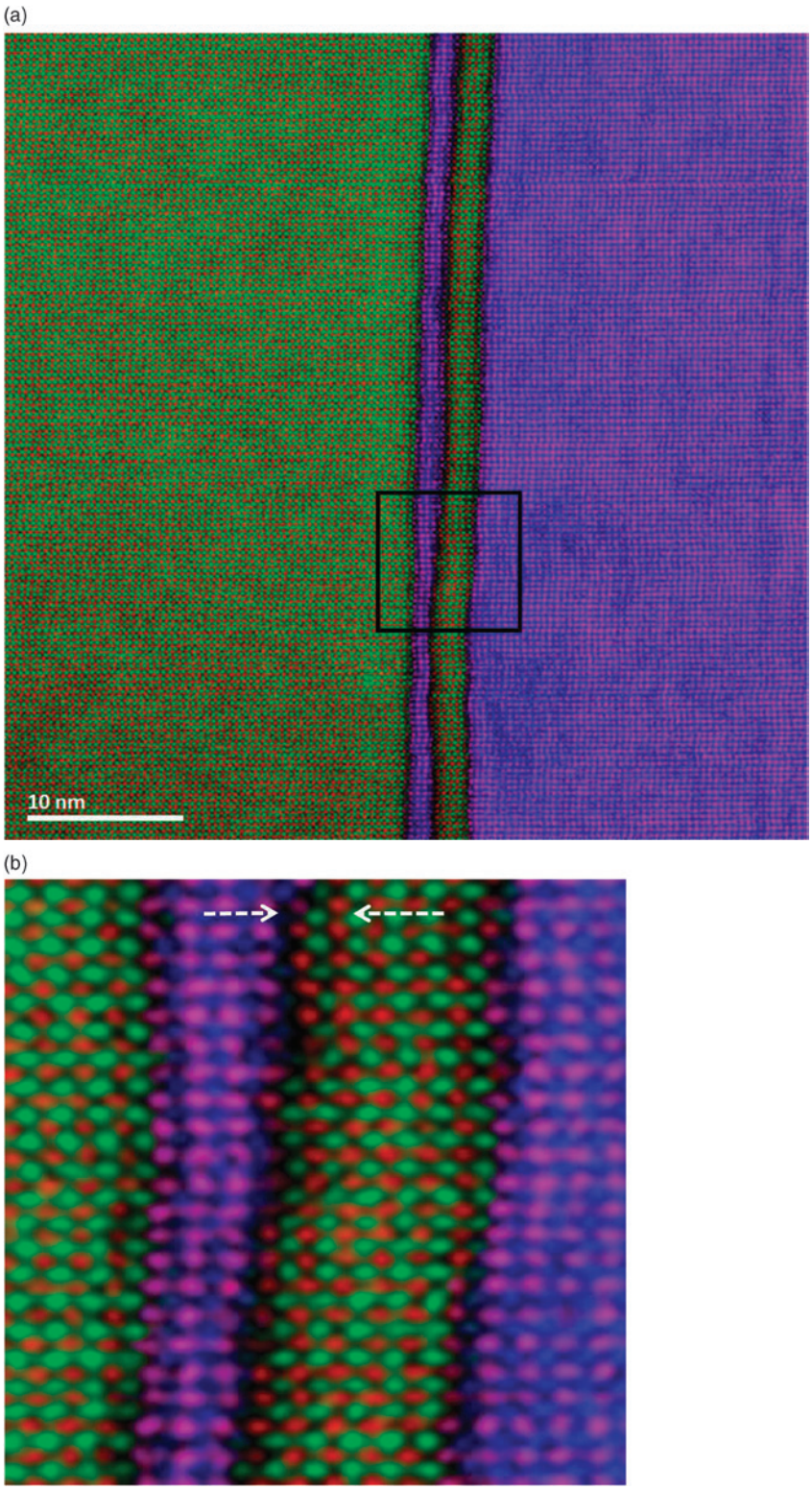

Figure 3: a) EELS colorized elemental maps across the STO/LMO/STO/LMO of Sr $L_{2,3}$-edges at 1,940 eV in red, Ti $L_{2,3}$-edges in green, Mn $L_{2,3}$-edges at 640 eV in blue, and La $M_{4,5}$-edges at 832 eV in purple. The contrast shown by these elemental maps is very high despite the short exposure time per spectrum. There is some roughness and elemental diffusion that can be observed across the interfaces. b) Enlarged view of the region in the black box of Figure 3a.

O K at 532 eV, Mn L at 640 eV, and La M at 832 eV), and data were extracted using MLLS fitting [3, 14, 15]. In the case of EDS, elemental maps were extracted using the X-ray lines for the same elements (Sr Lα at 1.81 keV, Ti Kα at 4.51 keV, O K at 0.52 keV, Mn Kα at 5.90 keV, and La Lα at 4.65 keV) using an empirical Kramers background subtraction followed by MLLS fitting of each peak family represented by a set of Gaussian peaks [16]. X-ray maps using the O K line were unsatisfactory because of the overlap between the O K and Ti L peaks, the low fluorescence yield, and absorption effects that strongly affect low-energy X rays [4,8,17].

Figures 4 shows the Ti, O, Mn, La, and Sr elemental maps obtained using EELS, whereas Figure 5 shows the same elemental maps taken with EDS X-ray signals. Qualitatively, there is less noise and higher contrast in all the EELS maps compared to those obtained using EDS. The O K elemental maps using EELS and EDS are shown in Figures 4b and 5b, respectively. The EELS data do not completely resolve individual oxygen atoms, but they do show the distributed oxygen framework. As mentioned above, the EDS data show no oxygen atom locations. Figures 6a and 6b show colorized elemental maps of Ti, Mn, La, and Sr and La obtained using EDS and EELS, respectively. The EELS map appears sharper and shows stronger contrast; the EDS data are noise-limited due to the low number of counts in each spectrum. It is important to note that the EELS and EDS data shown are the raw output and have not been filtered or de-noised.

Investigating chemistry across the interface. EELS can provide chemical bonding information when analyzing the core-loss region of the EELS spectrum. Bonding and coordination influences the shape of the near-edge fine structure and can shift the edge threshold energy resulting in a so-called chemical shift. These advantages are countered by the presence of plural scattering that can blur the shape of the near-edge structure and energy drift that prevents accurate measurements of the small chemical shift. Both these problems can be corrected using the low-loss spectrum acquired under the same conditions as the core-loss spectrum [3, 9, 10]. This acquisition capability is called DualEELS and allows nearly simultaneous collection of different regions of the EELS spectrum under the same experimental conditions.

To analyze compositional and bonding changes in this sample, data were acquired at higher energy resolution from the interface region using DualEELS mode. The spectrometer was configured with a dispersion of 0.25 eV/channel to give a measured energy resolution of 0.75 eV but an energy range from 0 to 900 eV (using DualEELS mode). This setup allows fine structure analysis of oxygen and transition metal

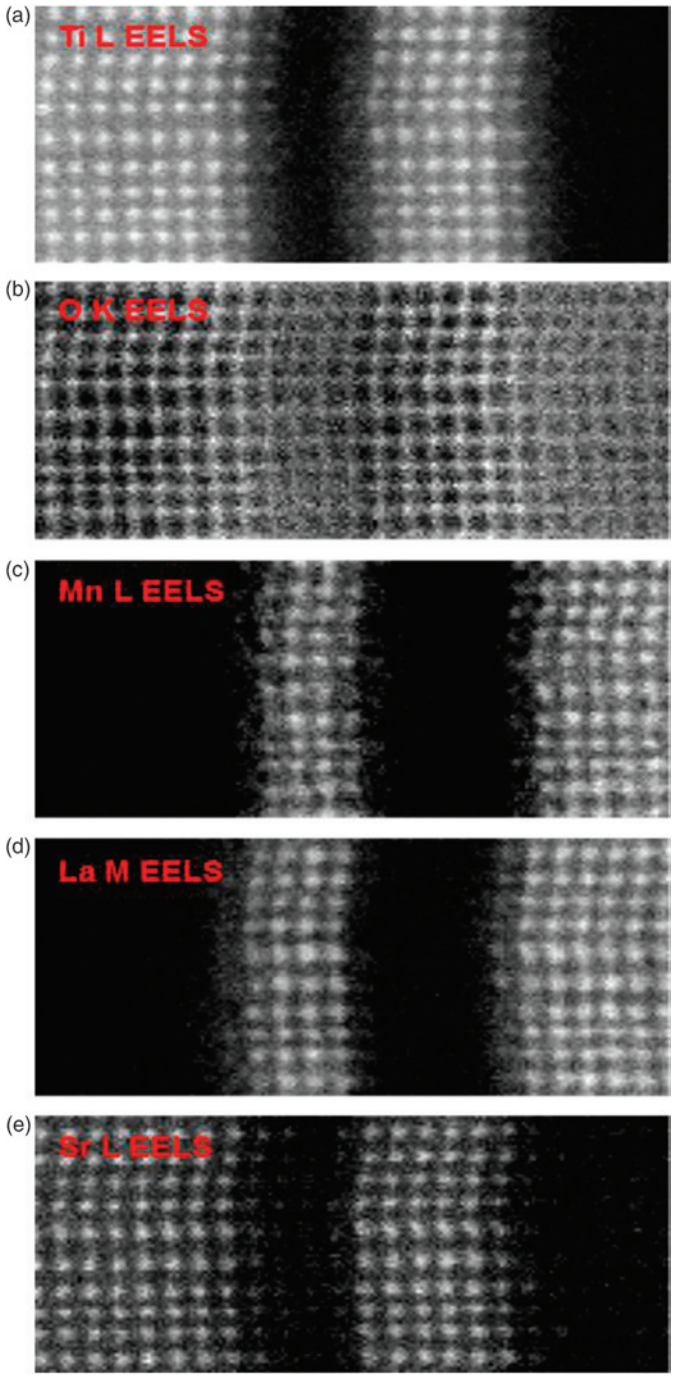

Figure 4: EELS elemental maps: a) Ti $L_{2,3}$-edges at 456 eV; b) O K-edge at 532 eV; c) Mn $L_{2,3}$-edges at 640 eV; d) La $M_{4,5}$-edge at 832 eV; and e) Sr $L_{2,3}$-edges at 1,940 eV.

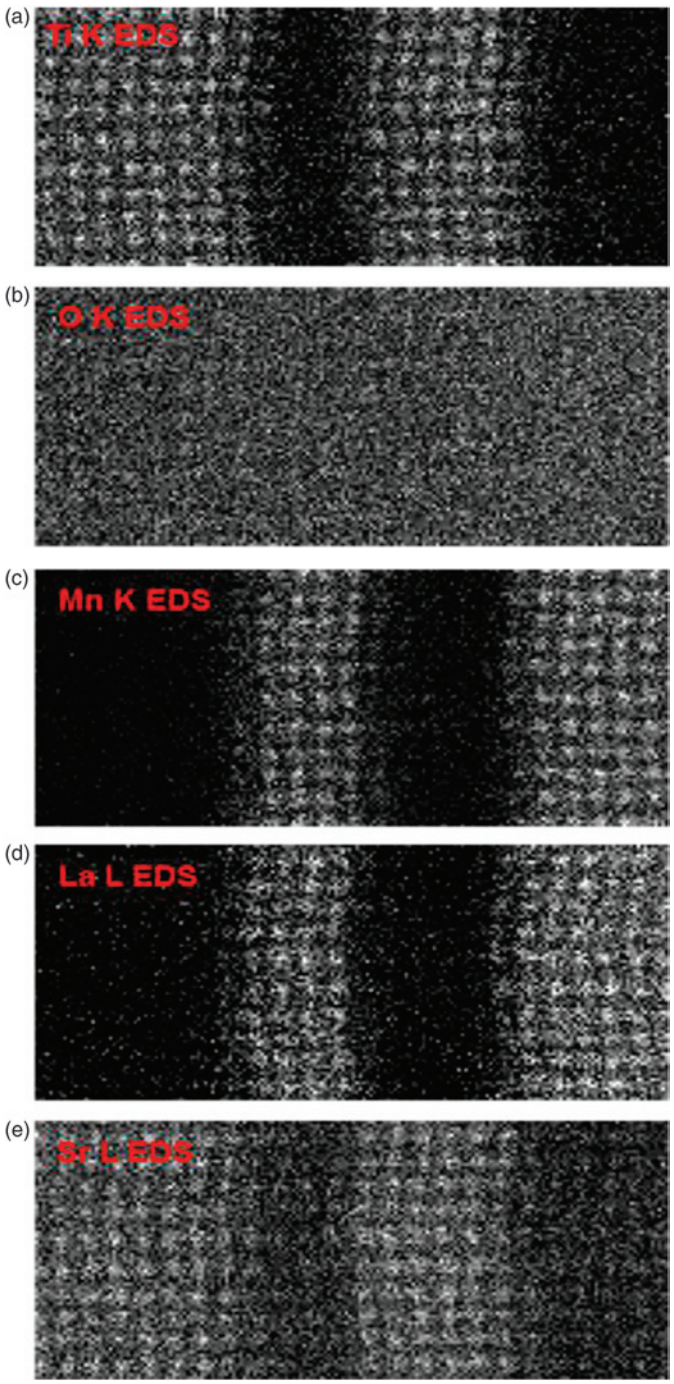

Figure 5: EDS elemental maps: a) Ti K lines at 4.51 keV; b) O K lines at 0.52 keV; c) Mn K lines at 5.90 keV; d) La L lines at 4.65 keV; and e) Sr L lines at 1.81 keV.

edges. The regions of the EELS spectrum from 0 eV to 500 eV and 400 eV to 900 eV were acquired nearly simultaneously with 10 µs transition time between exposures of 0.037 ms and 25 ms, respectively. The EDS data were recorded over the total pixel time of the DualEELS acquisition. The entire 160×45 pixel spectrum imaging dataset was taken in just 3 minutes.

Given the energy range allowed by this experiment, only the Ti-L, O-K, Mn-L and La-M edges were analyzed from the EELS data. The Sr-M edge at 130 eV was recorded but provides low SNR maps because of the high background in this region of the EELS spectrum [18], and the Sr L-edge at 1,940 eV was beyond the energy window in this setup. Because EDS data was acquired simultaneously, the Sr intensity could be monitored from the EDS line at 1.81 keV. This map can then be combined with those obtained by EELS. The EDS data only deliver compositional information, thus chemical and bonding information was available only for Ti, O, Mn, and La.

Composition maps at this high-energy resolution configuration were extracted from the area across the interface in

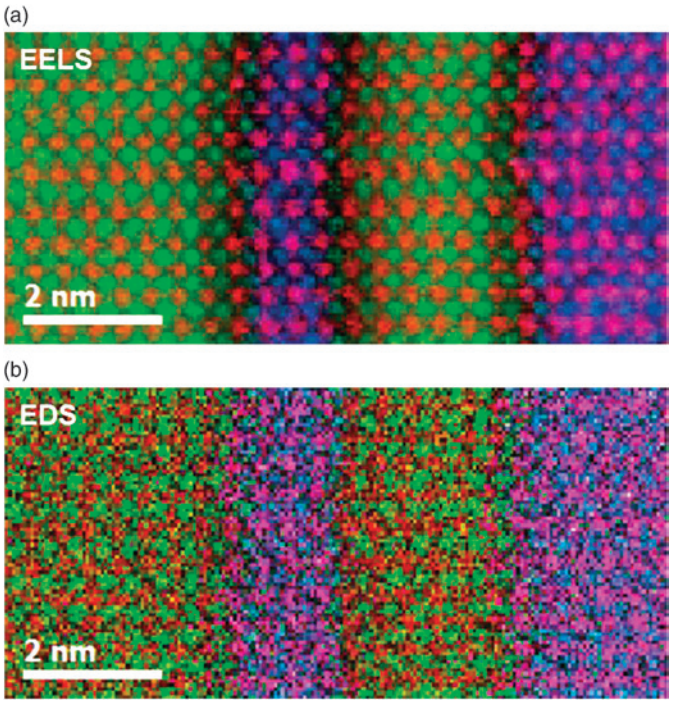

Figure 6: Colorized elemental maps of Ti in green, Sr in red, Mn in blue, and La in purple acquired using a) EELS and b) EDS.

the upper region of the ADF STEM image in Figure 1. The EELS and EDS maps were acquired using the method outlined in the previous section. Figure 7 shows the Ti, O, Mn, and La composition maps obtained using EELS, as well as a Sr composition map obtained using EDS. These elemental maps were combined to generate the composite color map in Figure 8 that shows the distribution of each element (oxygen is omitted for clarity). The intermixing across the interface that is also observed in the EELS compositional maps in Figures 3 and 6a, can now be further investigated by looking at changes in the fine structure of Ti, O, and Mn that occur across the interface region.

Figure 9 shows high-energy resolution EELS spectra of the Ti $L_{2,3}$-edges, O K-edge, and Mn $L_{2,3}$-edges extracted from the selected regions in Figure 8 across the STO/LMO/STO interfaces. Each spectrum is normalized to the same maximum and then vertically shifted for better visualization. Changes in the fine structure can be observed in every spectrum, although they are quite strong in the case of the O K-edge in Figure 9b. Here, the shape goes from that typical of $SrTiO_3$ to something intermediate with that of $LaMnO_3$. The pre-peak in the O K edge at 529 eV is due to the excitation of the electrons from the O 1s state to the partially filled O 2p state, which can be partially hybridized with 3D states of the transition metal. The size of this pre-peak is related to the strength of the hybridization with the transition metal, which varies as a result of different coordinations of the bonded atoms. In this case, O atoms in the same column are bonded to both Mn and Ti atoms. The effects of such intermixing can be seen in the O K-edge fine structure at the interface.

As shown in Figure 9a the Ti $L_{2,3}$-edges in the EELS spectrum splits into two sets of different peaks between

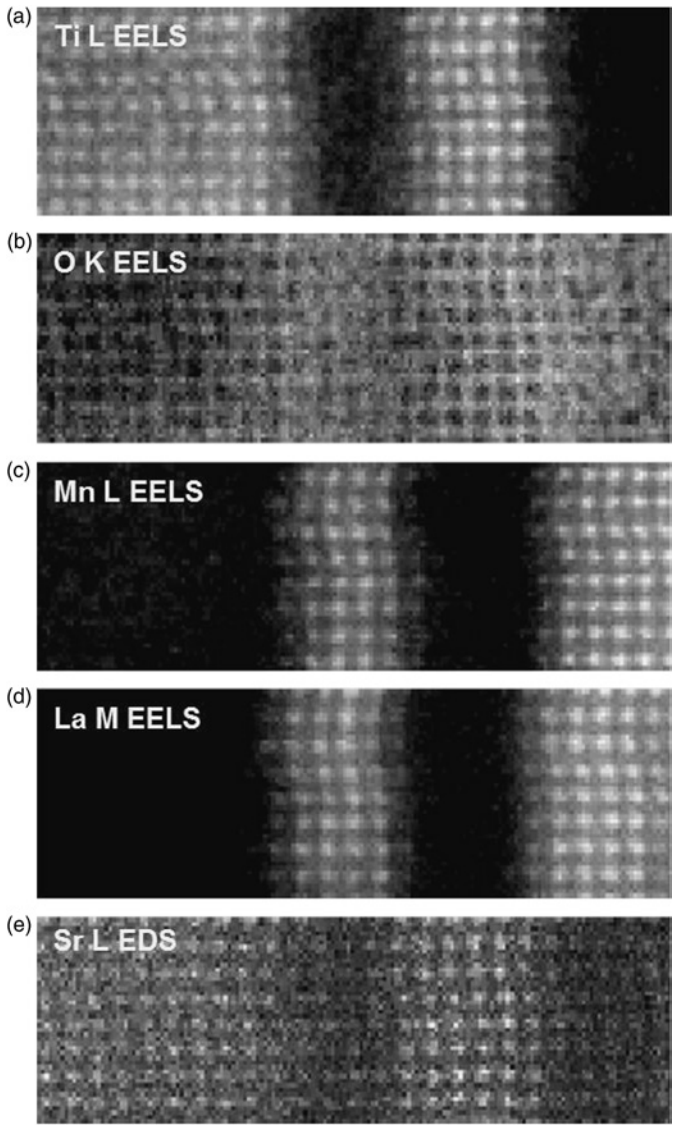

Figure 7: Ti, O, Mn, La, and Sr. a) EELS using the Ti $L_{2,3}$-edge at 456 eV; b) EELS using O K-edge at 532 eV; c) EELS using the Mn $L_{2,3}$-edges at 640 eV; d) EELS using the La $M_{4,5}$-edges at 832 eV; and e) EDS using the Sr L at 1.81 keV. Here the EELS spectrometer was set up with high dispersion in order to increase the energy resolution for the fine structure analysis. As a result, the field of view is reduced and extends up to 900 eV. Thus, the Sr $L_{2,3}$-edges at 1,940 eV are out of the field of view.

456 eV and 466 eV that can be labeled as L_3- and L_2-edges, respectively. They correspond to electronic transitions from the 2p3/2 and 2p1/2 core levels to a 3D excited state. Both edges are divided into t_{2g} and e_g bands whose relative intensities reflect the different distortions of the local coordination environment, and, coupled with simulations, they can be used to detect crystal distortion or changes in the oxidation state. As shown in Figure 9a there is the presence of Ti across the entire LMO layer, but the shape of Ti $L_{2,3}$-edges remains largely unchanged showing the features typical of Ti 4+. This indicates that the Ti atoms tend to keep their configuration largely unchanged going from the STO to the LMO layers. As mentioned above, the ZLP was used to correct for energy drift effects that usually occur as result of microscope or environmental instabilities. In this way the

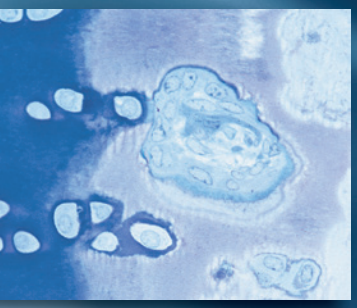

DiATOME

diamond knives

the highest quality...
the most precise sectioning...
incomparable durability

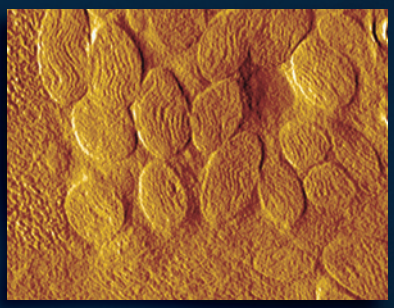

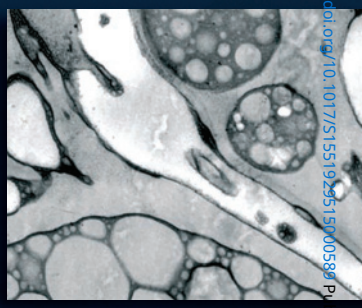

building on 40 years of innovation

ultra 45° • cryo • histo • ultra 35°
histo jumbo • STATIC LINE II • cryo immuno
ultra sonic • ultra AFM & cryo AFM

NEW!... trimtool 20 and trimtool 45
Finally, one trimming tool for all of your trimming needs, be it at room or cryo temperatures.

DiATOME U.S.

P.O. Box 550 • 1560 Industry Rd. • Hatfield, Pa 19440
Tel: (215) 412-8390 • Fax: (215) 412-8450
email: sgkcck@aol.com • stacie@ems-secure.com
www.emsdiasum.com

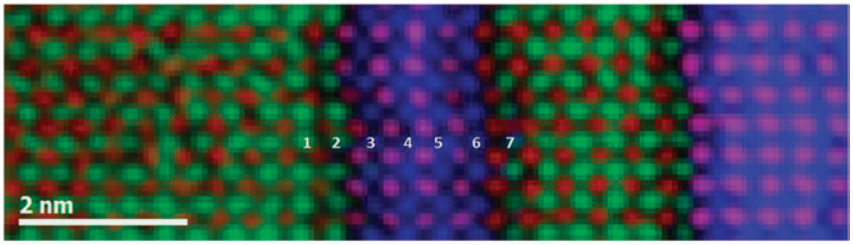

Figure 8: Colorized representation of the elemental maps in Figure 7 using Ti L in green, La M in purple, and Mn L in blue obtained using EELS, and Sr L in red obtained using EDS. The numbers 1–7 correspond to the selected region where the EELS spectra in Figures 9a–c were extracted.

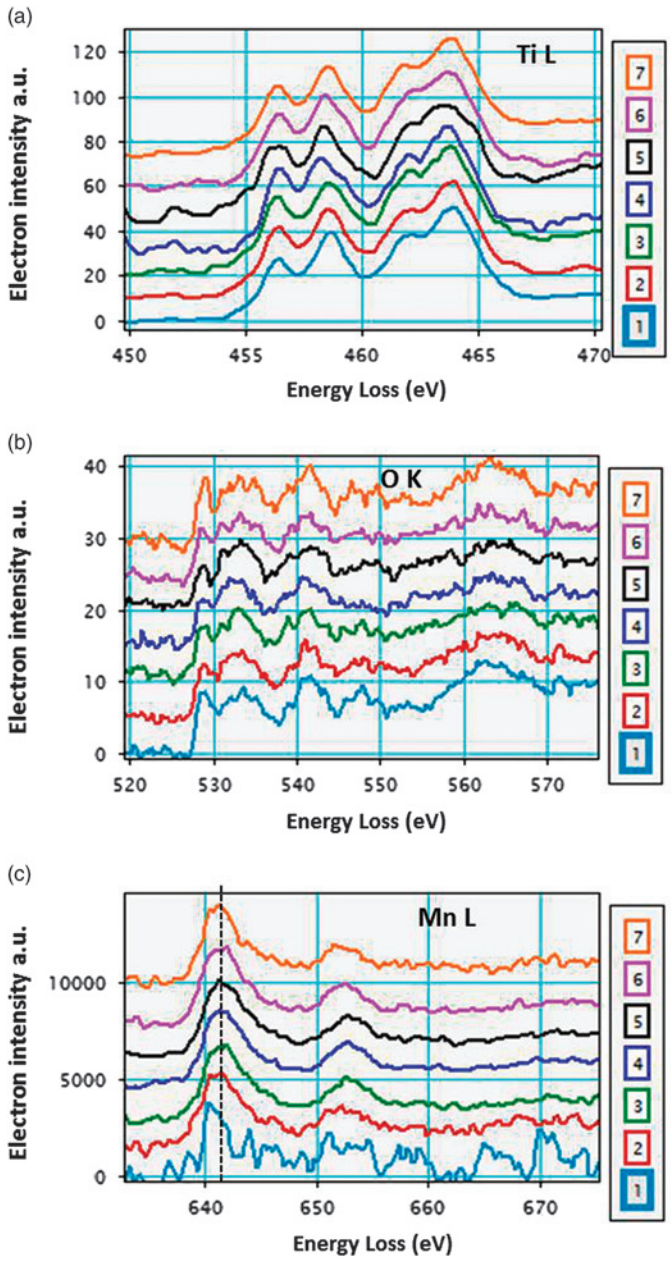

Figure 9: a) Ti $L_{2,3}$, b) O K, and c) Mn $L_{2,3}$ EELS data extracted from the selected region in Figure 8. All the spectra were normalized to same maximum in intensity and vertically offset for better visualization.

true chemical shift can be observed as shown in Figure 9c where the Mn $L_{2,3}$-edges for the spectra in position 1 and 2 are slightly shifted at lower energy.

Discussion

The EELS and EDS data presented here can be regarded as highly complementary. The main difference is that for the EDS case, each pixel carries little information because of the low signal-to-noise ratio of the data, even at relatively long acquisition times and with elements of high fluorescence yield. The high signal-to-background ratio of the EDS technique, however, allows summation of adjacent data almost indefinitely, which improves detection limits at the expense of spatial resolution. The EELS system, on the other hand, exhibits a high signal-to-noise ratio for each pixel because of the high collection efficiently of the EELS. Summing adjacent pixels improves the detection limits here also but will show diminishing returns once the shot noise in the signal integral becomes irrelevant. The techniques further complement each other when identifying artifacts in the data. For example, secondary fluorescence and preferential absorption in the EDS data can be determined from the EELS data, while possible missing elements in the EELS data range acquired can be identified in the summed EDS signal.

A system for fast and efficient acquisition of both EELS and EDS spectra allows the routine collection of both of these complementary signals. There is no longer a need to choose between analytical techniques; both EELS and EDS can be acquired easily with every data run. The data presented here show the complementary nature of having both high signal-to-noise and high signal-to-background data acquired at the same location at the same time. Further, the ability of combining composition measurements from EELS and EDS with physical and electronic information also available only from EELS (for exmaple, plasmonic, bandgap, and density of states information) [19] promises to open whole new avenues of materials analysis.

Conclusion

EELS and EDS are complementary analysis techniques that can, in the best environmental settings, provide elemental analysis at the level of atomic columns. Large-area EELS spectrum images can display atomic-level details of element locations from areas up to 2,500 nm^2. Simultaneous collection of detailed EELS and EDS elemental maps provides information about TEM thin specimens that is difficult or impossible to obtain by other means. Chemical bonding effects at the atomic column level can be detected when EELS setup parameters are adjusted for acquisition at the highest energy resolution.

References

[1] OL Krivaneck et al., *Ultramicroscopy* 96 (2003) 229–37.
[2] S Pennycook, *Microsc Anal* 26(6) (2012) 59–64.
[3] P Longo et al., *Microsccopy Today* 20(4) (2012) 30–36.
[4] P Longo et al., *Microscopy Today* 21(4) 2013) 36–40.
[5] P Schlossmacher et al., *Microscopy Today* 18 (2010) 14–20.
[6] PJ Phillips et al., *Microsc Microanal* 20 (2014) 1046–52.
[7] IOP Publishing. *Nanotechweb.org*, "EDX detects single atoms," http://nanotechweb.org/cws/article/tech/50459.
[8] P Longo et al., *Microscopy Today* 21(1) (2013) 28–33.
[9] AJ Gubbens et al., *Ultramicroscopy* 110 (2010) 962–70.

[10] J Scott et al., *Ultramicroscopy* 108 (2008) 1586–94.
[11] P Longo et al., *Microsc Microanal* 20 (2014) 779–83.
[12] A Pakzad. Gatan Inc., "Argon Ion Polishing of Focused Ion Beam Specimens in PIPS II System," Application note, 2014, http://info.gatan.com/acton/attachment/11413/f-0122/1/-/-/-/-/AppNote%20PIPS%20II%20Argon%20Ion%20Polishing%20FL1.pdf.
[13] S Lazar et al., *Microsc Microanal* 16 (2010) 416–24.
[14] K Riegler and G Kothleitner, *Ultramicroscopy* 110 (2010) 1004–13.
[15] P Longo. Gatan Inc., Application Note, 2011, "The use of MLLS fitting approach to resolve overlapping edges in the EELS spectrum at the atomic level," http://info.gatan.com/acton/attachment/11413/f-01a1/1/-/-/-/-/Use_of_MLLS_fitting_EELS_FL1.pdf.
[16] E Lifshin. *Proc 9th Ann Conf Microbeam Anal Soc*, Ottawa, Canada, 1974, paper no. 53.
[17] R Van Grieken and A Markowicz, *Handbook of X-ray Spectrometry*. Marcel Dekker, Inc., New York, 2001.
[18] GA Botton et al., *Ultramicroscopy* 110 (2010) 926–34.
[19] RF Egerton, *Electron Energy-Loss Spectroscopy in the Electron Microscope*, 2nd Edition, Plenum Press, New York, 1996.

MT